Imaging photothermal microscopy for absorption measurements of optical coatings

Chunxian Tao (陶春先)[1,2*], Yuanan Zhao (赵元安)[1], Hongbo He (贺洪波)[1], Dawei Li (李大伟)[1], Jianda Shao (邵建达)[1], and Zhengxiu Fan (范正修)[1]

[1]*R and D Center for Optical Thin Film Coatings, Shanghai Institute of Optics and Fine Mechanics, Chinese Academy of Sciences, Shanghai 201800, China*

[2]*Graduate University of Chinese Academy of Sciences, Beijing 100049, China*

[*]*E-mail: taochx@siom.ac.cn*

Received November 14, 2008

For absorption measurement of large-aperture optical coatings, a novel method of imaging photothermal microscopy based on image lock-in technique is presented. Detailed theoretical analysis and numerical calculation are made based on the image photothermal technique. The feasibility of this imaging method is proved through the coincidence between the theoretical results of single spot method and multi-channel method. The measuring speed of this imaging method can be increased hundreds of times compared with that of the raster scanning. This technique can expand the applications of photothermal technique.

OCIS codes: 310.0310, 120.0120.

doi: 10.3788/COL20090711.1061.

Photothermal spectroscopy is a group of high sensitivity spectroscopy techniques used to measure optical absorption and evaluate thermal characteristics of optical coating samples. The basis of photothermal spectroscopy is the change in thermal state of the sample resulted from the absorption of laser irradiation. In optical coating absorption detecting, surface thermal lensing (STL)[1] has been successfully used in weak absorption measurement achiving a result low to the order of ppm (its theoretic sensitivity is about 10 ppb). It is performed with a lock-in amplifier as the signal analyzer to obtain the alternating current (AC) component induced by the modulated coating absorption at single-spots. Meanwhile, the combination of absorption measurement with laser conditioning has been established and put into practical application[2]. This is rather helpful for local defect detection and damage threshold prediction of optical coatings[3−7].

In traditional STL, only one spot is irradiated at a time and detected by a lock-in amplifier. With the help of translation stage, the interested area can be scanned point by point, namely raster scanning. However, there are some fatal limitations to its application in large-scaled optical coatings. Firstly, the time spent is so long even to the unacceptable extent for practical operation. Secondly, the used devices, such as a YAG laser, cannot always keep in a steady state during the whole detection. Therefore, it would be desirable to have as many detection processes as possible done with lines parallel to each other at a time.

The lock-in technique has been used in thermography and optical coherence microscopy for infrared (IR) thermal image and topography imagery[8,9]. In this letter, a method of imaging photothermal detection based on image lock-in is presented and the microscopy is configured to implement the absorption measurement of large-aperture optical coatings.

The imaging detection uses photothermal theory combined with charge coupled device (CCD) camera to extract the signal of inhomogeneities (thermal defects) from the homogeneous bulk of the material (background signal). The block diagram of the multi-channel detection system is shown in Fig. 1. Its basic idea is to change from the synchronous detection using lock-in amplifier to the synchronous excitation[10].

There are four major functional units in the diagram named light sources, STL, async-modulator, and signal recorder. The light sources includes pump beam and probe beam. The STL unit means the surface thermal lens due to the coating absorption of the pump light. The key units for image lock-in are the async-modulator as shown in Fig. 2. Compared with the single channel detection, the pump beam and probe beam are both modulated by choppers. We adopt extended pump light and probe light to detect the larger area of an optical coating sample, instead of the single-spot heating and detecting of single channel method in Fig. 2(a).

The term of "image lock-in" is derived from the conception of phase lock-in theory, which is based on the correlation function of the signal and a reference at a specified frequency and phase relationship. The realization of image lock-in is illustrated in Fig. 3. The signal s of coating absorption is arising from a harmonic modulation at a frequency of f. It is a mixture of time-variant signal and background signal, in

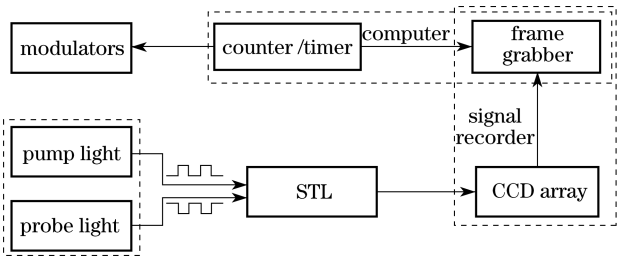

Fig. 1. Multi-channel lock-in detection block diagram.

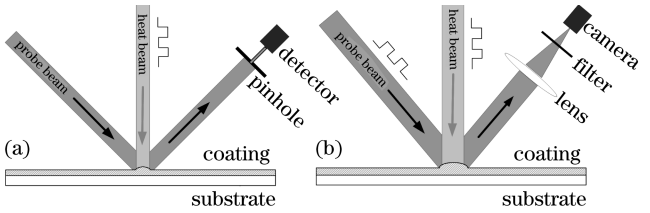

Fig. 2. Schematic configurations of (a) single channel and (b) multi-channel detection.

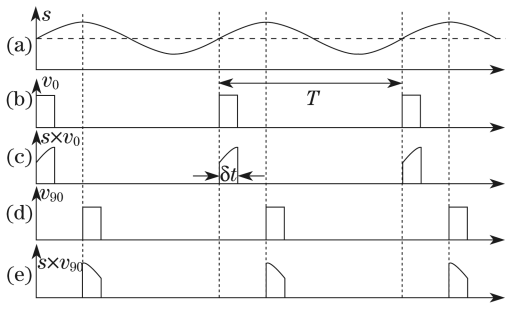

Fig. 3. Image lock-in process at 0° and 90°.

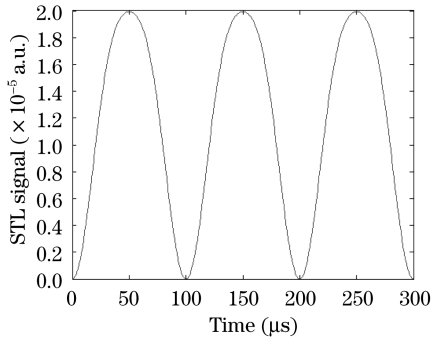

Fig. 4. Time dependence of coating absorption in sinusoidal modulation.

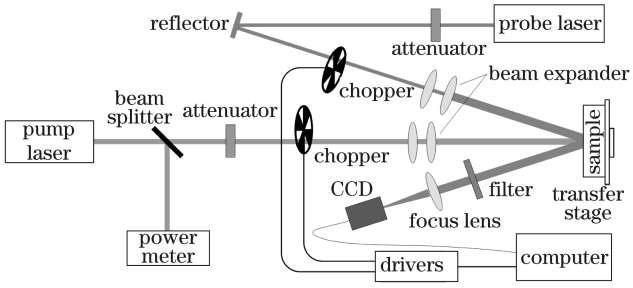

Fig. 5. Configuration of multi-channel photothermal microscopy.

which the former is concerned to the coating absorption while the latter is the direct current (DC) component of the reflected light. To accomplish the lock-in, the reference signal v_0 is introduced by modulating the probe light. These two signals have the same frequency but with changeable phase, as shown in Fig. 3(b, d). Similar to homodyne detection, once the two frequencies are equal to each other, the discernible phase of the periodic vibration is locked. The lock-in process at phase shift $\Delta\phi$ = 0° and 90° is illustrated in Figs. 3(c) and (e), respectively.

At the point of $r(x,\ y)$ of the sample, the diffraction signal s of the probe light passing through the STL can be expressed as

$$s\,(r,t) = A\mathrm{e}^{\mathrm{i}(2\pi ft+\phi_0)}, \tag{1}$$

where A and ϕ_0 denotes the amplitude and initial phase, respectively. This expression has been proved to be valid in the linear response scope of coating absorption in single channel detecting mode, as illustrated in Fig. 4. The photothermal images from the heated area are recorded by an area array CCD camera. Thus the recorded image is

$$S_{k,n}\,(r) = \frac{1}{\delta t}\int_0^{\delta t} S\,(r,t)v_0\,(\phi_{k,n})\,\mathrm{d}t. \tag{2}$$

The image lock-in system gives an in-phase image and an quadrature image by setting the reference signal v_0 in the form of $\sin(2\pi ft)$ and $\cos(2\pi ft)$. Generally, these results can be obtained by four-point algorithm. In this algorithm, the phase shift $\Delta\phi\,(t)$ between s and v_0 is expressed as

$$\Delta\phi\,(t) = \phi_{k,n} - \phi_0 = 2k\pi + n2\pi/4,$$

where $\phi_{k,n},\ \phi_0$ is the initial phase of the probe light and signal light, respectively. k and n are both integers, and k means the cycle number and n the sample sequence of 0 to 3. The CCD camera acts as a low-pass filter and integrates the signals in pulse width δt over N periods, producing a value S_n(r) as

$$S_n\,(r) = \frac{1}{k}\sum_{k=0}^{k-1} S_{k,n}\,(r),\ n = 0,\ 1,\ 2,\ 3. \tag{3}$$

According to the four-point correlation algorithm, the in-phase and quadrature phase signals are enough to accomplish the image lock-in process in harmonic modulation. The in-phase and quadrature signals from $S_0, S_1,\ S_2$, and S_3 are obtained by setting the phase shift at 0°, 180°, 90°, and 270° respectively. And thus the absorption signal can be reconstructed from these four recorded signals, which is expressed as

$$v_s = \sqrt{(S_0 - S_1)^2 + (S_2 - S_3)^2}, \tag{4}$$

$$\theta_s = \arctan\left(\frac{S_0 - S_1}{S_2 - S_3}\right). \tag{5}$$

There are three advantages of four-point correlation algorithm. First, the algorithm is more noise-immune. Second, it can be performed on-line during measurement. Third, the phase is insensitive to quadratic nonlinearities. All of these features fully meet our measurement requirements. This lock-in detection can also be performed on other points of the heated sample simultaneously. Therefore, the distribution of the whole field heat defects on the optical coating can be generated.

The configuration of the multichannel photothermal microscopy is established according to Fig. 5. The YAG continuous laser at 1064 nm and He-Ne laser at 632.8 nm

Table 1. Experimental Parameters

Detection Mode	Probe waist radius W_0 (μm)	$W_{\rm probe}$ (μm)	$W_{\rm pump}$ (μm)	$R_{\rm bump}$ (μm)
Raster Mode	20	596.6	40	100
Multi-Channel	20	596.6	40	100
Multi-Channel	20	596.6	80	100
h_0 (nm)	$\lambda_{\rm probe}$ (nm)	$d_{\rm sw}$ (mm)	$d_{\rm sd}$ (mm)	f (Hz)
4	632.8	−59.2	300	10
4	632.8	−59.2	300	10
8	632.8	−59.2	300	10

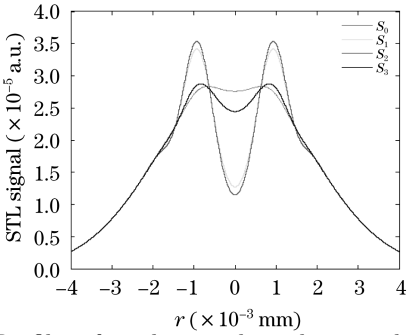

Fig. 6. Profiles of in-phase and quadrature phase signal.

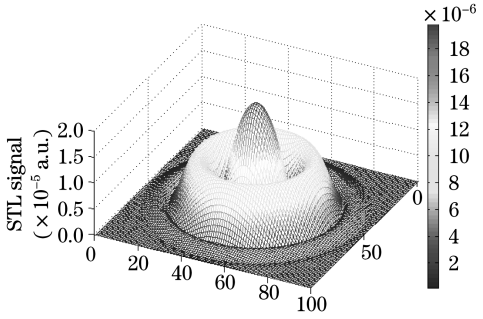

Fig. 7. Three-dimensional image of constructed photothermal signals.

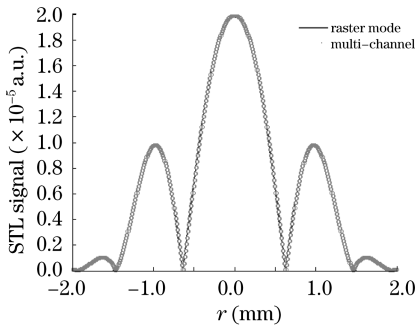

Fig. 8. Results comparison between image mode and single mode.

are used as the pump light and probe light. The pump beam has an output of 30 W and a maximum of 20 mW of which reaches the sample controlled by an attenuation system. The attenuator is composed of two sets of polarizer and quarter-wave plate in which a precious range of regulation can be realized up to between 0.01% and 100%. The modulators unit is composed of two sets of electronic shutter driven by two specified pulse sequences, which are both generated by the counter/timer card. A multi-pixel CCD is used at an acquisition speed of 30 frame/s.

The feasibility of the multi-channel measurement of coatings absorption is analyzed and demonstrated through theoretical calculations based on the Fresnel diffraction principle. The theoretical values of the absorption signal at stimulated area are calculated in image method and raster scanning method, respectively. The experimental parameters are listed in Table 1.

Profiles of the diffracted photothermal images in phase and quadrature states are illustrated in Fig. 6, where the solid, dash, dotted, and solid-dotted lines represent S_0, S_1, S_2, and S_3, respectively. Based on Eq. (3), the constructed photothermal image is calculated as shown in Fig. 7. From this figure, it is known that the deformed area induced by the defect absorption is distinguished from the area without heat stimulation. Evidently, the image lock-in has been realized by cancelling the static image from that affected by the laser stimulating. Consequently, only the AC signal of $v_{\rm s}$ induced by the coating absorption is picked from the total image. Moreover, this operation also eliminates random noise imposed on the signals, such as scattering light and dark current of the CCD.

The calculated results of coating absorption at single defect spot in image mode (line) and single-spot mode (dash) are illustrated in Fig. 8. It is found that the theoretical result in image mode coincides with that of the single-spot mode in this spot. In traditional STL, the coating absorption is fully characterized by the value of the central peak. The coincidence of the two results demonstrates that the image lock-in technique can totally fulfill the requirement of imaging measurement and defects detection.

The applied heat and probe beam in imaging detection are extended by a laser beam expander to detect larger area of the sample. The baseline of laser intensity for effectively stimulating a defect limits the extended diameter of the heat beam. The relationship between the signal and the diameter of the probe and pump beam are illustrated in Figs. 9 and 10. Generally, the central signal is the largest to be used as the effective signal for absorption analysis. As shown in Fig. 9, the central signal increases with the increase of the diameter of the probe beam. This means that the diameter of the probe beam may not be as important be as that of the pump one, as long as it is the larger of the two.

However, the variation of the signal with the increase of the pump diameter is much more complicated, where two extreme points separate the curve into three parts. According to the curve diagram in Fig. 10, a proper radius of the pump beam can be set to 500 μm. In addition, there is a wider value range of pump beam radius proper for imaging detection.

Generally, the time used in absorption measurement of film coatings depends on the scale of the detected spot and the step length during raster scanning in STL technique. In the image method, the heat area of the coating can be extended up to 500 μm or even larger. Consequently, the measuring time is dramatically reduced for

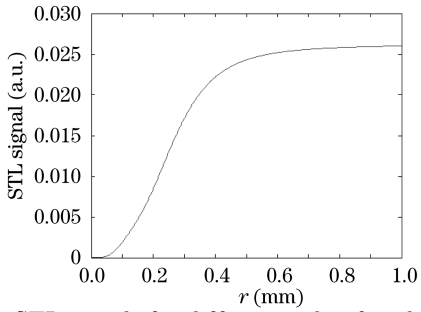

Fig. 9. STL signals for different radii of probe beam.

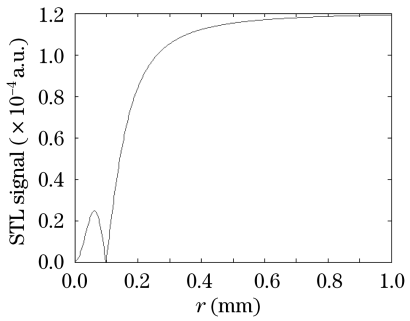

Fig. 10. STL signals for different radii of pump beam.

large-aperture film coatings. Taking consideration of the adjustment time and post process, the theoretical speed of data acquisition is about several hundred times as much as that of the raster scanning mode.

In summary, we suggest a non-destructive surface characterization method for optical coating quality control. The imaging STL technique offers an opportunity to obtain the full-field information of the surface defects and thus significantly reduces the diagnostic time for large-aperture coatings. A good signal to noise ratio can be achieved in use of the image lock-in technique, which improves the spatial resolution of the heat absorption distribution. This photothermal microscope is practicable for identifying defects and potential laser damage sites for laser conditioning on large scale optical coating components.

This work was supported by the National Natural Science Foundation of China under Grant No. 60708004.

References

1. R. Chow, J. R. Taylor, and Z. L. Wu, Appl. Opt. **39,** 650 (2000).
2. L. Gallais and M. Commandré, Appl. Opt. **45,** 1416 (2006).
3. Z. Wu, C. J. Stolz, S. C. Weakley, J. D. Hughes, and Q. Zhao, Appl. Opt. **40,** 1897 (2001).
4. B. Bertussi, J.-Y. Natoli, and M. Commandré, Appl. Opt. **45,** 1410 (2006).
5. Z. L. Wu, P. K. Kuo, Y. S. Lu, S. T. Gu, and R. Krupka, Thin Solid Films **290-291,** 271 (1996).
6. C. Xu, H. Dong, J. Ma, Y. Jin, J. Shao, and Z. Fan, Chin. Opt. Lett. **6,** 228 (2008).
7. C. Wang, Z. Han, Y. Jin, J. Shao, and Z. Fan, Chin. Opt. Lett. **6,** 773 (2008).
8. O. Breitenstein, M. Langenkamp, F. Altmann, D. Katzer, A. Lindner, and H. Eggers, Rev. Sci. Instrum. **71,** 4155(2000).
9. A. Dubois, A. C. Boccara, and M. Lebec, Opt. Lett. **24,** 309 (1999).
10. E. Beaurepaire, A. C. Boccara, M. Lebec, L. Blanchot, and H. Saint-Jalmes, Opt. Lett. **23,** 244 (1998).